RSC Advances

ROYAL SOCIETY OF CHEMISTRY

www.rsc.org/advances

RSC Advances RSCPublishing

ARTICLE

Graphene oxide interpenetrated polymeric composite hydrogels as highly effective adsorbents for water treatment

Cite this: DOI: 10.1039/x0xx00000x

Received 00th January 2014,
Accepted 00th January 2014

DOI: 10.1039/x0xx00000x

www.rsc.org/

Chong Cheng,[a,b] Zhengyang Liu,[a] Xiaoxiao Li,[a] Baihai Su,[c] Tao Zhou,[a,*] and Changsheng Zhao,[a,*]

Recent studies showed that polymeric hydrogels presented promising applications in adsorption to various water contaminants. However, the usages of these synthetic hydrogels are hindered by several inherent shortages, e.g. limited inner porosity, low adsorption capacity and long equilibrium time. In this study, synthetic GO interpenetrated poly(acrylic acid) (PAA) hydrogels as 3D high-efficient adsorbents were prepared and systematically studied for the first time. The mediating ability of GO on inner structure and adsorption capacities is examined by two types of PAA hydrogels (PAA1 and PAA2 with different inner structures, prepared by in-situ cross-linked polymerization of monomer AA). The results indicated that the prepared PAA2/GO hydrogels owned well-defined and interconnected 3D porous network, which allowed the adsorbate molecules to diffuse easily into the absorbent. The adsorption experiments indicated that the obtained interconnected polymeric composite hydrogels could efficiently remove cationic dyes and heavy metal ions from wastewater; the highest adsorption capacity of the prepared PAA2/GO composite hydrogels could reach as high as 1600 mg/g, which present great promising in treatment of environmental toxins. Moreover, the initial concentration, pH value, desorption ratio, dynamic kinetics and isotherms of methylene blue (MB) adsorption processes of the prepared PAA2/GO composite hydrogels were also studied in detail. The experimental data of MB adsorption fitted the pseudo-second-order kinetic model and the Langmuir isotherm very well, and the adsorption process was controlled by the intraparticle diffusion. Moreover, due to its facile preparation and low-cost, the GO interpenetrated PAA composite hydrogels may function as promising adsorbents for the wastewater treatment; and this method might also be extended to improve the adsorption capacity of other polymeric hydrogels.

1. Introduction

Nowadays, the widespread use of chemical compounds and hazardous materials around the world has led to serious water pollution, especially the industrial dyes, heavy metal ions and other toxic molecules, which may lead to retention toxicosis, lethal poison and carcinogenic contact to human beings and animals even at ultralow concentrations.[1] As a result, the removal of the toxic molecules from industrial wastewater, such as methylene blue (MB), methyl violet (MV), Cu^{2+} and Pd^{2+}, has become a critical issue.[2] Various approaches to remove toxic molecules from water have been explored and developed.[3, 4] Among them, adsorption has gained importance as a purification and separation technique in industrial scales and becomes an attractive option for industrial water treatment, especially the removal of organic compounds that are chemically and biologically stable.[5] Till now, it has been reported that clays,[6-9] hydrophobic porous polymers,[10] various organic-inorganic composites, and polymeric hydrogels[11] could selectively remove water pollutants. Among these materials mentioned above, polymeric hydrogel is one of the most promising adsorbents due to their facile preparation, low-cost, and high-specific loading capacity.[12, 13] Recently, various synthetic polymer based hydrogels have been fabricated,[14, 15] such as poly(acrylic acid) (PAA) and polyacrylamide hydrogels, these obtained hydrogels demonstrated certain adsorption capability as effective adsorbent for various contaminants. However, the usage of these synthetic polymer engineered hydrogels also face several inherent shortages, e.g. limited porosity, low adsorption capacity and long equilibrium time.[16]

Thus, it has been found that various nano-additives could further improve the adsorption capacity and porosity of polymeric hydrogels, such as nanofibers[17] and carbon nanotubes,[18, 19] which may function as dispersing agents to increase the interconnected porous structures of polymeric composite adsorbents.[20, 21] Meanwhile, recent works have revealed that the added nanomaterials could not only effectively improve the loading capacity and also shorten the adsorption time.[22] However, the high-cost fabrication process and complex steps needed for the preparation of these nano-additives may limit these obtained polymeric composite hydrogels from applications as fast and efficient adsorbents. Graphene oxide (GO), consisting of monolayer structure with oxygen functional groups, such as carboxyl groups, hydroxyl groups, is one of the most important derivatives of graphene.[23] The single layer structure endows GO sheets with ultra-large specific surface area and highly negative-charged surface, which endow GO as ideal candidate as the nanocarriers, such as the drugs, gene, and other molecules.[24-26] Zhang et al.[27] studied the MB adsorption by aqueous dispersed single layer GO, and the adsorption capability was as high as 1750 mg/g. Therefore, it is expected that GO could act as the interpenetrating agent and adsorption additive to effectively improve the porosity and adsorption capacity of synthetic polymer hydrogels.[27] Meanwhile, GO could be produced from cheap graphite via simple chemical oxidation routes, which made GO become ideal low-cost nano-additives for preparation of interpenetrated composite hydrogels.[28]

Recently, numerous researches have been carried out to explore the environmental applications of GO and GO based composite adsorbents, these composite materials revealed outstanding adsorption capacities against various toxic compounds in aqueous solution.[29-35] Shi et al. prepared the graphene oxide/sodium alginate/polyacrylamide ternary nanocomposite hydrogel with excellent mechanical performance and also good adsorption properties for water-soluble dyes.[36] Our group had assembled the biopolymer mediated graphene oxide hydrogels as efficient and multifunctional adsorbents, which owned excellent blood compatibility and thus conferred the hydrogels with great potentials for various blood-contact applications.[37] Zhao et al. prepared poly(acrylamide) (PAM) polymer brushes on chemical reduced GO sheets for the adsorption of heavy metals and benzenoid compounds.[38] PAA, as one of the most important polyanion, owned excellent adsorption capacity and also could form hydrogel easily via crosslinking polymerization method. It would be very interesting and industrial promising to fabricate and investigate the GO/PAA hydrogel adsorbents. Most recently, several methods had been applied to prepare the PAA/GO composite hydrogels, while, in these studies the GO was barely applied to reinforce mechanical and thermal properties of the composite hydrogels.[39-42] Using GO as dispersing or interpenetrating agents to improve the interconnected porous structures and corresponding adsorption capacity of polymeric PAA hydrogels have not been explored. GO had been proved to be super-amphiphile with hydrophilic edges (ionized carboxyl groups) and a more hydrophobic basal plane (polyaromatic islands of unoxidized sp^2 carbon skeleton). GO could act like a surfactant, owned adsorption ability on the interfaces and could lower the surface or interfacial tension.[43] Small size GO acted as molecular surfactant and large size GO behaved like molecule-colloid dualistic surfactant. Thus, due to this surfactant or colloidal property, after mixing and polymerization with AA monomer, the GO might adsorb the monomers and regulate the polymerization process, thus dispersing the crosslinked PAA polymer chains, and preventing the formation of thick walls and non-interpenetrated pore structure. Futhermore, GO nanosheets were found to be able to covalent grafting with the polymerized PAA polymer chains, thus functioned as the backbone/skeleton of the formed hydrogels,[44] thus resulted in porous inner structure due to its large surface area and nanosheet structure. Thus, GO can be regarded as the dispersing or interpenetrating agents, it was highly necessary and meaningful to clarify the GO influence on the inner structure and adsorption process of the PAA/GO composite hydrogels, and the relationship between the interconnected porous structure and adsorption capacity should also be systematically explored.

Here, in this study, synthetic GO interpenetrated PAA hydrogels as 3D high-efficient adsorbents were prepared and systematically studied for the first time. To investigate the mediating ability of GO and the corresponding adsorption effects of different interpenetrating structures in composite hydrogels, two types of PAA hydrogels (PAA1, PAA2) with different kinds of inner structures were prepared by *in-situ* polymerization of monomer AA and cross-linkable monomer N,N'-methylene bisacrylamide (BIS) firstly; the different inner structures are mediated by changing the content of the initiator and reaction temperature. The GO interpenetrated PAA composite hydrogels were prepared by a similar *in-situ* polymerization in the presence of GO nanosheets. Then, the change of the inner structures and the adsorption performances before and after adding GO with two type of PAA hydrogels were observed and compared. The morphology and porosity changes of the hydrogels were observed by scanning electron microscope (SEM) and Brunauer–Emmett–Teller (BET). Methylene blue (MB) molecule was chosen as the model adsorbates to exam the influence of inner interpenetrated structure on the adsorption performances of the prepared hydrogels. The adsorption capacity of the prepared PAA2/GO composite hydrogels can reach as high as 1600 mg/g, which present great promising in various adsorptions of environmental toxins. To reveal the application potential of the PAA2/GO composite hydrogels, the adsorption capability, kinetics and equilibrium isotherms of MB for the GO interpenetrated PAA2 hydrogels were systematically investigated. Compared to the earlier adsorption studies by using polymeric hydrogels, this study demonstrated that GO could function as the interpenetrating agent to improve the porosity and inter-connectivity, and the interpenetrated inner structure could advance the adsorption capacity of polymeric hydrogels. The obtained hybrid hydrogels exhibited a controllable 3D porous

morphology and ultrahigh loading capacity of hazardous molecules, which might satisfy industrial environmental applications due to their large-scale and low-cost by means of a facile technique; and this method might also be extended to improve the adsorption capacity of other polymeric hydrogels, such as polystyrene sulfonate (PSS), PAM, and etc.

2. Experimental

2.1 Materials

Monomer, acrylic acid (AA), initiator (ammonium persulfate, APS) and cross-linking agent (N,N'-methylene bisacrylamide, BIS) were purchased from Aladdin reagent Co. Ltd. (China) with analytical grade and used as received. Graphite flakes were purchased from Sigma-Aldrich. The adsorbates used in this study (MB, MV, Cu2+, and Pb2+) are purchased from Aladdin reagent Co. Ltd. (China). All the aqueous solutions were prepared with de-ionized water (DI water).

2.2. Preparation of PAA hydrogels and PAA/GO composite hydrogels

In a typical process, poly (acrylic acid) hydrogels were prepared by in-situ polymerization of monomer AA and cross-linking agent BIS in the presence of 2.13 mg APS, and polymerized at 70 °C for 4 h, and termed PAA1; the detailed components are showed in Table 1. The PAA1 hydrogels showed less connected inner structure with lower adsorption capacity, which will be discussed in the results part. To prepare the hydrogel with high inner porous structure, PAA2 hydrogel was synthesized by increasing the amount of APS (26 mg) and the polymerization temperature at 80 °C. The higher APS concentration and reaction temperature might facilitate the inner interpenetrated structure of the hydrogel, thus increasing the adsorption capacity. After the polymerization, the hydrogels were purified in distilled water for at least 4 days to remove residual monomers and initiator, and then freeze-dried.

Table 1 The synthetic chemical components and surface areas of PAA1 and PAA2 hydrogels.

Materials	AA (g)	BIS (mg)	APS (mg)	Water (g)	$S_{BET}(m^2.g^{-1})$
PAA1	0.52	26	2.13	10	13.23
PAA2	0.52	26	26	10	68.43

After PAA1 and PAA2 hydrogels are obtained, the GO are applied to prepare PAA/GO interpenetrated composite hydrogels via a similar process. GO nanosheets were prepared via the modified Hummers method according to a previous work with a minor modification;[45] the chemical structure of GO was confirmed by Atomic force microscopy (AFM) and Transmission electron microscope (TEM) images, as shown in Fig. S1.[46] The PAA/GO interpenetrated composite hydrogels were prepared by in-situ polymerization of monomer AA and cross-linkable monomer BIS in the presence of GO nanosheets. The synthetic chemical components of PAA1/GO composite hydrogels are shown in Table S1. The composite hydrogels of PAA2/GO are prepared as shown in Table 2. Typically, 5 g GO solution (6 mg/g) was added into 3 g water to obtain A solution, 26 mg BIS, 26 mg APS and certain amount of AA monomer were dissolved in 2 g water to form a mixed B solution; then the A and B solutions were mixed together with vigorous agitation at N_2 protection to obtain a homogenous mixture. Then, the reaction was conducted at 80 °C for 4 h.[47] For the sake of comparison, different ratios of PAA2/GO are obtained; the components of the different hydrogels are showed in Table 2. The hydrogels with 43%, 15%, and 6% GO/AA ratio were named as PAA2-GO-3 , PAA2-GO-2, and PAA2-GO-1, respectively. The 43% GO/AA ratio was set as the highest GO ratio in this system due to the stability of the hydrogels in the adsorption experiment; further increasing the GO/AA ratio would result in unstable hydrogels. The photographs of the prepared PAA2 and PAA2/GO interpenetrated hydrogels and the gelation formation test are shown in Fig. S1.

Table 2 The synthetic chemical components and surface areas of PAA2/GO composite hydrogels.

Materials	AA(g)	BIS(mg)	APS(mg)	Water(g)	GO(mg)	GO/AA(%)	$S_{BET}(m^2.g^{-1})$
PAA2	0.52	26	26	10	0	0	68.43
PAA2-GO-1	0.52	26	26	10	30	6	73.25
PAA2-GO-2	0.20	26	26	10	30	15	85.43
PAA2-GO-3	0.07	26	26	10	30	43	100.15

Pure PAA1, PAA2, PAA1/GO and PAA2/GO composite hydrogels were lyophilized for morphological studies and adsorption experiments. The morphologies of the hydrogels were observed by Field-emission scanning electron microscope (SEM, FEI Sirion-200, USA). For the SEM observation, the hydrogels were freeze-dried to constant weight, and then cut by a single-edged razor blade after immersing into liquid nitrogen. Thereafter, the prepared samples were attached to the sample supports and coated with a gold layer before observation. BET–N_2 experiments were carried out by using auto-porosity analyzer (Micromeritics TriStar 3000, USA). All the hydrogels were degassed overnight at 160 °C prior to adsorption experiments. Zeta potential measurements of the aqueous dispersions for the PAA/GO hydrogels were performed using Zetasizer ZS90 (Malvern Instruments Ltd, UK).

2.3. Adsorption experiments

In order to investigate the adsorption capacity of the PAA hydrogels and PAA/GO composite hydrogels, 1 mg lyophilized hydrogel was applied in 50 mL methylene blue (MB) solution (100 μmol/L) at the temperature of 25±1 °C and pH value of 6.6. The MB concentration was determined at different time intervals with an UV-vis spectrometer (UV-1750, Shimadzu Co., Ltd, Japan) at the wavelength of 631 nm with the pre-established calibration curve. The data were also used for adsorption kinetics study.

For the PAA2/GO composite hydrogels, the effect of the initial concentrations on adsorption was also studied. 1 mg PAA2-GO-2 hydrogels were applied to 50 mL MB solutions with the initial concentrations of 50, 100, 150, and 200 μmol/L, respectively. The concentrations were also determined at

different time intervals and the data were also used for analyzing adsorption isotherms and adsorption kinetics of the obtained PAA2/GO hydrogels.

To study the effect of pH value on the adsorption of cationic molecules, the pH values of MB solutions (100 μmol/L) were controlled at 3, 5, 6.6, and 9 by adding hydrochloric acid or sodium hydroxide solutions, other conditions (amount of composite hydrogel, volume of solution and stirring speed) were maintained the same, and the experimental temperature was 25±1 °C. The concentrations of these solutions were determined when equilibrium was reached by an UV-vis spectrometer.

The PAA2 and PAA2/GO hydrogels that reached adsorption equilibriums in MB solutions of 100 μmol/L were then chosen optionally for discussing the desorption ratio. The desorption experiments were carried out as follows: after the adsorption completed, the dehydrated hydrogels were applied into hydrochloric acid solutions (pH=2) or ethanol solutions, then stirred for 2 minutes and kept them stand still. After 24 hours, the concentrations of the MB in the hydrochloric acid solutions or ethanol solutions were determined, and the solutions were replaced by the fresh ones for the next desorption process. This process was repeated for three times until the desorption was completed. In each time, the desorption ratio (R_d) was obtained as:

$$R_d = \frac{n_d}{n_a} \times 100\%$$

Where n_d is the desorbed amount of the MB into the solution at each time; n_a is the adsorbed MB amount by the hydrogels, which is calculated from the adsorption experiment. The total desorption ratios are the sum of the R_d for the three repeating times.

At last, the adsorption capabilities to the other organic dyes, MV, and heavy metal ions (Pb^{2+}, Cu^{2+}) were also tested. For MV adsorption, the PAA2 and PAA2/GO hydrogels were applied in 50 mL 100 μmol/L MV solutions in glass tubes at 25±1 °C, pH 6.6. The concentrations of the solutions were determined after 72 h when the adsorption reached the equilibrium. For heavy metal ions adsorption, the concentrations of Pb^{2+} and Cu^{2+} ions were determined by using an atomic absorption spectrometer and all the initial concentrations were 1 mmol/L. We examined the removal capacity of heavy metal ions to prove that the PAA2/GO composite hydrogels could reduce heavy metal pollution in water as well.

3. Results and discussion

3.1. Characterization of PAA hydrogels and PAA/GO composite hydrogels

To investigate the GO mediated interpenetrating structure on the adsorption capacities of polymeric hydrogels, two types of PAA hydrogels with different kinds of inner structures and initial adsorption capacities were prepared by in-situ cross-linked polymerization at different conditions, and then the inner structures and adsorption performances were observed and compared. As shown in Fig. 1a and b, the PAA1 (a1-a3) hydrogel presents barely any interconnected structure, and the pore wall in the hydrogel is very thick, which is ranged from 300 nm to 800 nm. While, for the PAA2 (b1-b3) hydrogels, porous inner structure was obviously observed, and the pore wall is very thin ranged from 45 nm to 50 nm with interpenetrated pores. The different inner pore structures might be resulted from the polymerization conditions; when increasing the amount of APS (26 mg) and polymerization temperature (80 °C), the polymerization speed of PAA will increased and also increase the formation speed of the hydrogel, thus less thick and less completed pore walls will be formed in the hydrogel. The higher APS concentration and reaction temperature might also facilitate the formation of the inner interpenetrated pores via generating gas bubbles. The BET results in Table 1 also indicated that the PAA2 hydrogels own higher surface area than PAA1. The different pore walls and inner interpenetrated structures may endow the PAA1 and PAA2 with dramatically difference in the adsorption capacities. Methylene blue (MB, 100 μmol/L solutions) was chosen as the model adsorbate to exam the adsorption performances of the prepared hydrogels. The prepared two types of PAA hydrogels with different wall thickness, porosity and interconnected structure were found own dramatically different absorption capacities. The highest adsorption capacity of the PAA1 hydrogel is only 65 mg/g, while that of the PAA2 hydrogel is as high as 750 mg/g. The dramatic difference in adsorption capacity between the PAA1 and PAA2 hydrogels was caused by the difference in the pore wall thickness and interconnected structure. Combined the SEM and the adsorption data, Fig. 1d presents the simulation images of inner structure transformation when the amount of APS and the polymerization temperature increased. The inner structures of the hydrogels transform from non-interpenetrated PAA1 to inner interpenetrated PAA2, which may present great benefit for the diffusion of MB molecules and increasing the availability of the carboxyl groups in the PAA2 hydrogel.

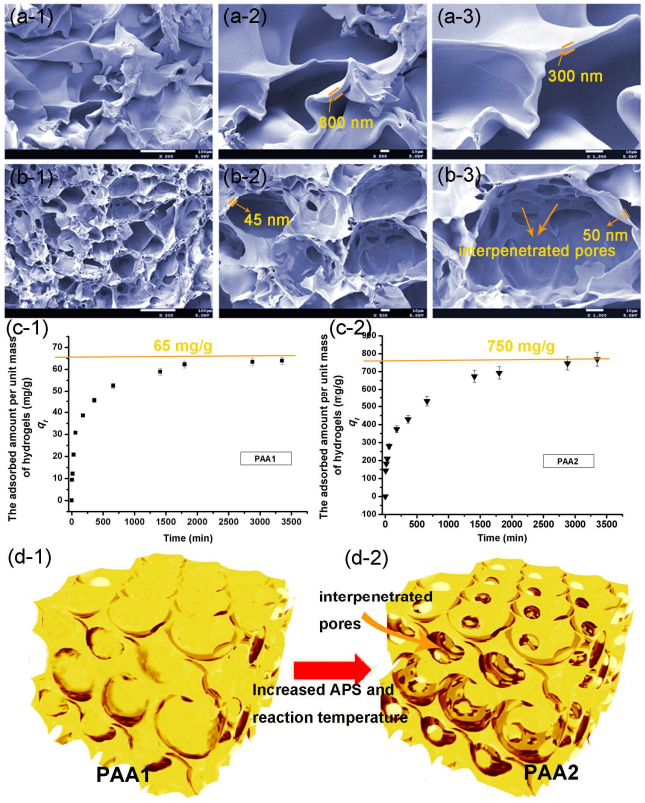

Fig. 1. The SEM images for the PAA1 (a1-a3) and PAA2 (b1-b3) hydrogels. The scale bars for a1-b1 are 100 µm, a2, a3, b2 and b3 are 10 µm. (c-1) The time-dependent MB adsorbed amount per unit mass of PAA1. (c-2) The time-dependent MB adsorbed amount per unit mass of PAA2. (d) The simulation images of inner structure difference: PAA1, non-interpenetrated structure; PAA2, inner interpenetrated porous structure.

Then, GO was added to the PAA1 and PAA2 hydrogels respectively to examine the mediating ability of GO for the inner porosity and interconnection of the PAA hydrogel. The GO interpenetrated PAA composite hydrogels were prepared by a similar in-situ polymerization in the presence of GO nanosheets. The enhanced interpenetrated structure was confirmed by SEM, and the data are shown in Fig. S2 and Fig. 2. For the PAA1/GO hydrogels, the PAA1-GO-1 and PAA1-GO-2 presented more porous structure than the PAA1. As indicated by the SEM in Fig. 2, after the addition of GO into the PAA2 hydrogels, the PAA2/GO composite hydrogels also become more porous than PAA2. The increased porosity had also been indicated by BET method in Table 2, the surface area increased from 68.43 to 100.15 $m^2.g^{-1}$ when GO was added; however, it was hard to detect the change of the pore size due to the complex pore size distributions of the composite hydrogels. More importantly, the pore wall becomes nanolayer structure with highly interpenetrated pores. Meanwhile, when increasing the GO ratio, the porosity and degree of the interpenetration of the PAA2/GO hydrogels increased gradually. The addition of GO nanosheet in the formation of hydrogel might facilitate the formation of nanolayer framework with abundant inner interpenetrated pores, thus make the hydrogel form completed interpenetrated inner structure, and the adsorbents in the hydrogel may become available.

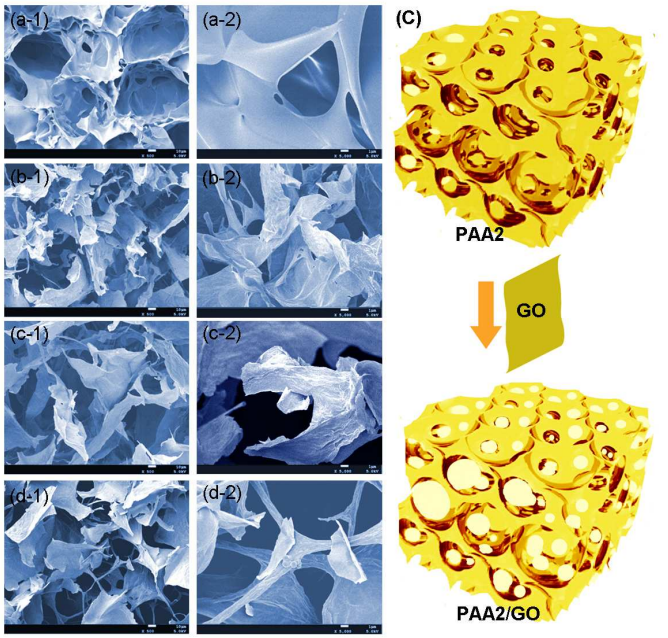

Fig. 2. The SEM images for the PAA2/GO hydrogels, inner structures for PAA2 (a-1) and (a-2); PAA2-GO-1 (b-1) and (b-2); PAA2-GO-2 (c-1) and (c-2); and PAA2-GO-3 (d-1) and (d-2). The scale bars for a1-d1 are 10 µm, a2-d2 are 1 µm. (c) The simulation images of the increased inner interpenetrated structure of PAA2/GO composite hydrogels.

Fig. 2c presents the increased inner interpenetrated structure of the PAA2/GO composite hydrogels after adding the GO nanosheets. The inner pores of the composite hydrogels become more interpenetrated than the PAA2, which could allow fast adsorption of MB molecules and increasing the availability of the adsorbates. To investigate the influence of the GO framework interpenetrated pores on the adsorption capacity of the hydrogels, the MB adsorption capacities of the prepared composite hydrogels were studied in detail. As shown in Fig. 3d, the prepared PAA2/GO hydrogels exhibited gradually increased absorption capacities when increasing the GO contents. The highest adsorption capacity of PAA2 hydrogel is 750 mg/g, while, the PAA2-GO-3 hydrogel can reach as high as 1600 mg/g. The significant increase of the adsorption capacity should be caused by the completely interpenetrated pore structure.

In a conclusion, the PAA1/GO and PAA2/GO hydrogels confirmed that GO could increase the inner interpenetrated structure and improve the adsorption capability of PAA hydrogel. It was found that the hydrogel network changed intensively after adding GO; meanwhile, the GO make more intensive morphology change for the PAA2 hydrogels than the PAA1 hydrogels. Except the morphology change, the adding of GO also affect the chemical structure of PAA2 hydrogels as indicated by the FTIR spectra in Fig. S4, the growth of PAA polymer chains was supposed to become more ordered due to its affinity with GO skeleton.

3.2. Adsorption of MB by the GO interpenetrated PAA2 hydrogels

The MB adsorbed amounts of the PAA2/GO composite hydrogels are shown in Fig. 3, the adsorbed amount increased with the increase of the GO mass ratios in the composite hydrogels. All the adsorption processes reached final equilibrium after about 60 h, the long equilibrium time might be caused by the multilevel porous structure of the composite hydrogel: because of the abundant interior micropores, the diffusion of adsorbates would take a long time. The equilibrium adsorbed amounts of MB for the hydrogels PAA2, PAA2-GO-1, PAA2-GO-2 and PAA2-GO-3 were 769.28, 809.07, 1003.78 and 1609.48 mg/g, respectively. The data also indicated that the increased mass of GO and the increased adsorbed amount did not fit linearity. These results might be attributed to that the utilization efficacy of PAA and GO nanosheets both increased when the GO mass increased. After adding GO, the PAA2/GO composite hydrogels could reach more than 80% adsorption capacity within 200 min, while, the PAA2 need more than 1000 min to reach 80% adsorption capacity.

The effect of initial concentration on the adsorbed MB amount to the PAA2/GO composite hydrogel was also investigated by using the PAA2-GO-2 as the model since the PAA2-GO-3 showed higher data variation as shown in Fig. S5. The adsorbed amounts of PAA2-GO-2 at various initial concentrations are shown in Fig. 3b. With the increase of the initial concentration, the adsorbed amounts to the PAA2-GO-2 increased. The maximum adsorbed amounts of MB at the concentrations of 50, 100, 150, 200 μmol/L, were 510.66, 1004.63, 1284.54, and 1678.94 mg/g, respectively. The increase of the maximum adsorbed amount could be attributed to the increased contacting probability between the MB molecules and the adsorbing sites in the composite hydrogel. Moreover, high concentration could accelerate the diffusion of the MB molecules into the composite hydrogel, thus decrease the adsorption equilibrium time.

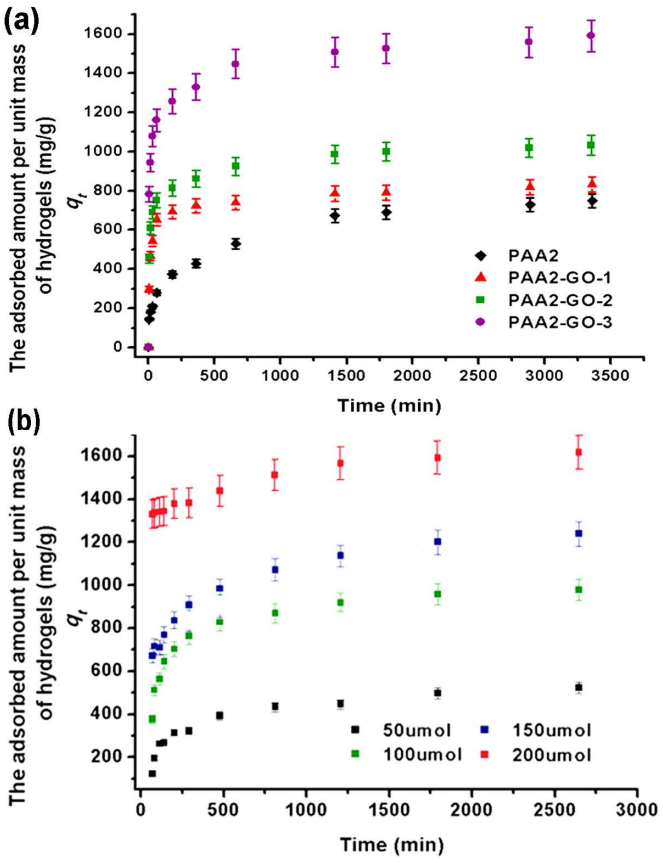

Fig. 3. (a) The time-dependent MB adsorbed amount per unit mass of PAA2, PAA2-GO-1, PAA2-GO-2, and PAA2-GO-3. (b) The time-dependent MB adsorbed amounts per unit mass of PAA2-GO-2 at various initial concentrations.

3.3. Effect of pH on the GO interpenetrated PAA2 hydrogels

The change of pH values of the solutions could change the surface charge of the PAA2/GO composite hydrogels. Thus, it might have a significant effect on the adsorbed amount of MB. Fig. 4a shows the Zeta potential of the PAA2/GO composite hydrogels at different pH values; Fig. 4b shows the relationship between the pH values of the solutions and the MB adsorbed amounts. For the Zeta potential, all the values of the hydrogels gradually decreased when the pH values increased, which indicated the surface charges of the hydrogels increased when increasing the pH values. For the MB adsorption, it was found that the adsorption capacities gradually increased with the increase of the pH values from 3 to 9. The change of the MB adsorption capacity should be resulted by the following reasons: at low pH value, a relatively high concentration of H^+, which competed strongly with MB cations for adsorption sites. Furthermore, the protonation of carboxyl and hydroxyl groups would lead to electrostatic repulsion, which would restrict the MB cations to come into close contact with the adsorbent surface.[48] When the pH value increased, the carboxyl and hydroxyl groups would deprotonate and form $–COO^-$ or $–O^-$ groups, which might enhance the electrostatic attraction between the adsorbent surface and MB cations. Consequently, the adsorbed amount of the composite hydrogel increased.

Furthermore, with the increase of pH values, the MB adsorbed capacity increased more dramatically for the PAA2-GO-3 than the PAA2-GO-2 and PAA2-GO-1. Thus, the GO content in the hydrogels presents an obvious impact on the adsorbing ability.

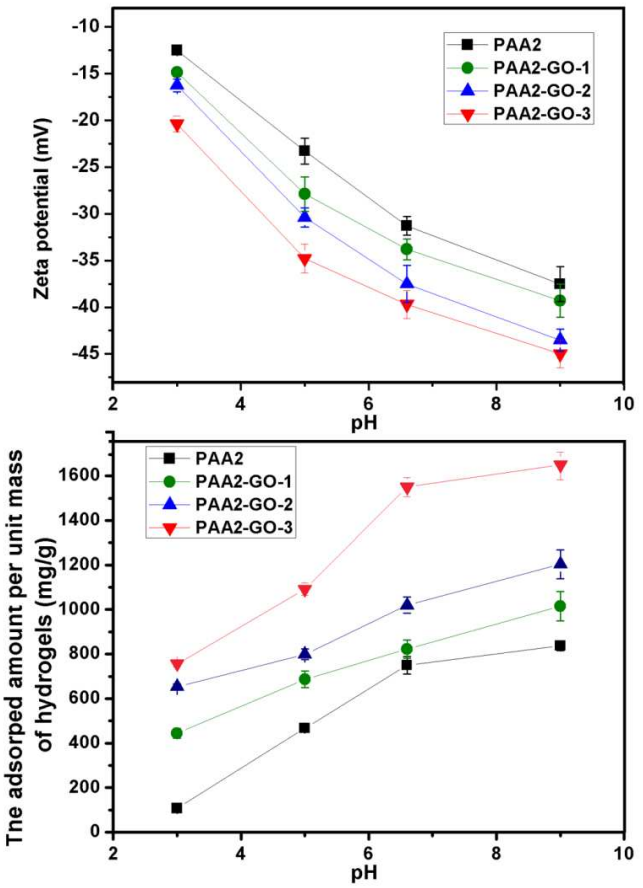

Fig. 4. (a) The Zeta-pH values for PAA2, PAA2-GO-1, PAA2-GO-2, and PAA2-GO-3. (b) Effects of pH values on the MB adsorption for PAA2, PAA2/GO-1, PAA2/GO-2, and PAA2/GO-3 composite hydrogels at the concentration of 100 μmol/L MB.

3.4. Desorption of MB from the PAA2/GO composite hydrogels

Hydrochloric acid solution (pH=2) and ethanol solution were used for desorption experiments. In each desorption process, the equilibrium adsorbed PAA2/GO composite hydrogels were used for desorption. When the rate of the desorption became slow, we replace the acidic solution or the ethanol solution with fresh one every 24 hours. The desorption ratios for different repeating times and different kinds of hydrogels are shown in Fig. 5. As shown in the figure, the desorbed ratios for the PAA2/GO composite hydrogels in the two solutions showed different tendencies.

In acidic aqueous solution, the desorbing ratios at the first desorption cycle for the PAA2/GO hydrogels were very high. The desorption ratios of MB were 80.44%, 76.08%, 82.96%, and 87.69% for PAA2, PAA2-GO-1, PAA2-GO-2, and PAA2-GO-3, respectively. For the second and the third desorption times, the desorbing ratios were both quite low, which indicated that most of the MB dyes could be removed by the first desorption process. For the desorption by ethanol, the desorbing ratios were much lower than those in acidic aqueous solution at the first cycle, and they were only 16.53%, 10.56%, 20.29%, 33.71% for PAA2, PAA2-GO-1, PAA2-GO-2, and PAA2-GO-3, respectively. In addition, the total desorbing ratios are less than 50% in ethanol solutions even after repeating 3 times. Thus, the total acid desorption ratios of the PAA2/GO composite hydrogels were much higher than those in ethanol solution, which indicated that the prepared composite hydrogels exhibited excellent desorbing efficiency in acidic aqueous solution, thus the PAA2/GO composite hydrogels could be reused after the adsorption.

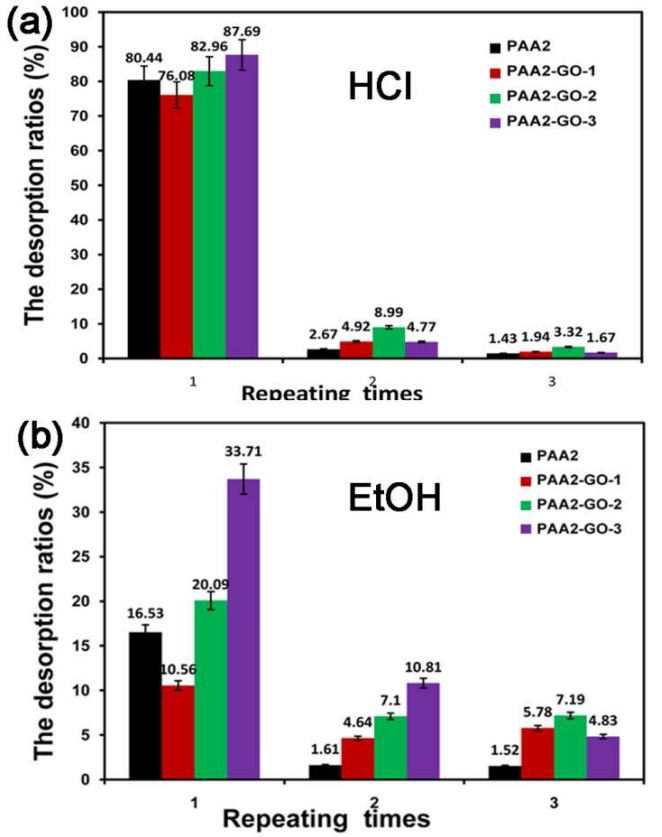

Fig. 5. (a) and (b) show the desorption ratios of the adsorbed MB in acidic aqueous solutions and ethanol solutions, respectively. The desorption process was repeated for three times, and each time continued 24h. Data are expressed as the mean ±S.D. of three independent measurements.

3.5. Adsorption kinetics study of PAA2/GO composite hydrogel

Since the PAA2/GO composite hydrogels revealed ultra-high adsorption capacities against toxic cationic molecules, and presented great potential in purification fields. Thus, the kinetics and isotherms of the adsorption processes of MB were studied in detail. To detect the detailed adsorption process and mechanism of these PAA2/GO composite hydrogels, three kinetic models were used to analyze the experimental data, i.e. the pseudo-first-order equation, the pseudo-second-order equation and the intraparticle diffusion equation.

3.5.1. The pseudo-first-order kinetic model

The pseudo-first-order kinetic model is more suitable for low concentration of solute. It can be written in the following form [49]:

$$\ln(q_e - q_t) = \ln q_e - k_1 t \quad (1)$$

where q_t is the MB amount adsorbed at time t (mg/g); q_e is that adsorbed at the equilibrium (mg/g); k_1 is the rate constant of pseudo-first-order equation. The plot of $\ln(q_e-q_t)$ against t should give a straight line with slope $-k_1$ and intercept $\ln q_e$, as can be seen in Fig. 6. The parameters are shown in Table 3, and the correlation coefficient values (r^2) of MB adsorption for PAA2, PAA2-GO-1, PAA2-GO-2, and PAA2-GO-3 composite hydrogels were 0.991, 0.824, 0.801, and 0.810, respectively. The calculated values of q_e were 782.89, 814.43, 1017.14, and 2354.56 mg/g, respectively, which were greater than the q_e that were obtained from the experiments (769.28, 809.07, 1003.78, and 1609.48 mg/g for PAA2, PAA2-GO-1, PAA2-GO-2, and PAA2-GO-3, respectively). The results indicated that the experimental data did not agree well with the pseudo-first-order kinetic model.

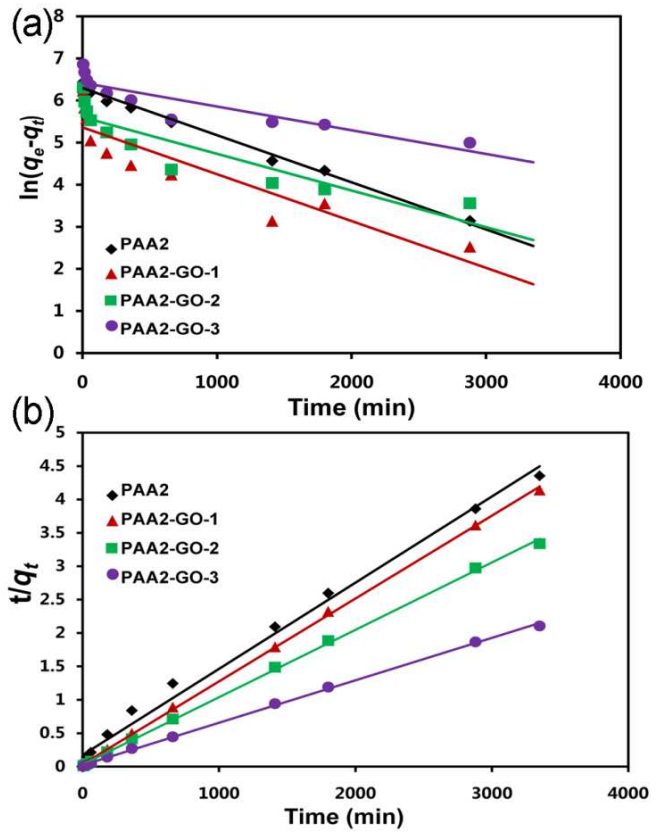

Fig. 6. (a) Application of the pseudo-first-order adsorption model for the adsorption of MB onto PAA2/GO composite hydrogel, (b) Application of the pseudo-second-order adsorption model for the adsorption of MB onto PAA2/GO composite hydrogel.

The pseudo-second-order equation is dependent on the amount of the solute adsorbed on the surface of adsorbent and the amount adsorbed at equilibrium. The pseudo-second-order model can be represented in the following form [50]:

$$\frac{t}{q_t} = \frac{1}{k_2 q_e^{\,2}} + \frac{t}{q_e} \quad (2)$$

where k_2 is the rate constant of pseudo-second-order equation, q_t, q_e, and t have the same meanings as those in pseudo-first-order equation. From the slope and intercept of the plot of t/q_t versus t which are shown in Fig. 6, the rate constant (k_2) and the equilibrium adsorption capacity (q_e) can be obtained. As seen in Table 3, all the correlation coefficients (r^2) were higher than 0.990, which meant that the adsorption of MB by the PAA2/GO composite hydrogel fitted the pseudo-second-order model very well. The calculated values of q_e were 769.23, 833.33, 1000.00, and 1666.67 mg/g, respectively, which were much closer to the experimental values than those in the pseudo-first-order model.

Table 3 The parameters of pseudo-first-order model and pseudo-second-order model for the adsorption of MB by the PAA2/GO composite hydrogels.

Composite hydrogel	$q_{e(exp)}$(mg/g)	Pseudo-first-order		Pseudo-second-order		
		$q_{e(cal)}$(mg/g)	r^2	k_2(g/mg·min)	$q_{e(cal)}$(mg/g)	r^2
PAA2	769.28	782.89	0.991	8.43×10^{-6}	769.23	0.993
PAA2-GO-1	809.07	814.43	0.824	4.10×10^{-5}	833.33	0.999
PAA2-GO-2	1003.78	1017.14	0.801	3.07×10^{-5}	1000.00	0.999
PAA2-GO-3	1738.78	2354.56	0.810	4.58×10^{-6}	1666.67	0.999

3.5.2. The intraparticle diffusion model

Besides using the pseudo-first-order and the pseudo-second-order equations to identify the adsorption process, considering that they could not identify the diffusion mechanism, the intraparticle diffusion model was used.[51, 52] The intraparticle diffusion equation can be written in the following form:

$$q_t = k_p t^{1/2} + C \quad (3)$$

where k_p is the rate constant of intraparticle diffusion model, C is a constant for any experiment (mg/g), q_t has the same meaning as that in Eq.(2). By plotting q_t versus $t^{1/2}$ the curves with three steps were obtained.

As seen in Fig. 7, the slope of the linear part of each curve could give the rate constants, from the extrapolation of the first step in the curves to the time axis, the intercepts C can be obtained. As seen in Table 4, the intercepts indicated that the boundary layer in the composite hydrogel impeded the intraparticle diffusion, and the adsorption process was rather complex; and the intraparticle diffusion was not the only rate-limiting step, most of the correlation coefficients (r^2) were higher than 0.95, which meant that the adsorption of MB by the PAA2/GO composite hydrogel fitted this model very well.

The three slopes in each curve indicated that there were at least three diffusion forms during the adsorption process: the external surface adsorption or diffusion in macro-pores occurred at the first step, until the exterior surface reached the saturation. The MB molecules entered into the less accessible pores, so the diffusion resistance increased and the diffusion rate decreased. The slope of the linear portion indicated the rate of the diffusion; a larger k corresponded to a faster diffusion

process. Hence, $k_1>k_2$, indicated that the free path for diffusion available became smaller and the pore dimensions decreased, thus leading to the reduced rate in the diffusion process. It can be seen from the figure that the first slopes of the PAA2/GO composite hydrogels are higher than that of PAA2; meanwhile, the k_1 increased with increasing the GO amount, which indicated that GO played an important role in the promotion of MB diffusion process in the composite hydrogels. Then, the second step, which was controlled by intraparticle diffusion, was the gradual adsorption step. The pace for this section is lower than the first step. The third step was the final equilibrium step, for which the adsorbent molecules moved slowly from larger pores to micropores and caused a slow adsorption rate. The interpretation of this phenomenon had also been reported by other literatures. [53 54]

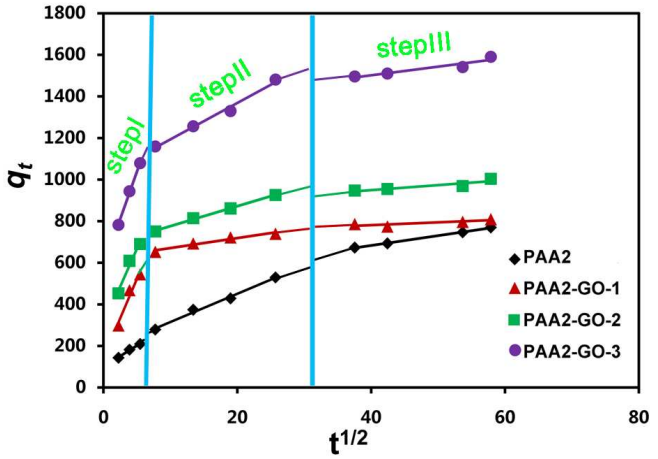

Fig. 7. Application of the intraparticle diffusion model for the adsorption of MB onto the PAA2/GO composite hydrogels.

Table 4 The parameters of intraparticle diffusion model for the adsorption of MB by the PAA2/GO composite hydrogels.

Composite hydrogel	C(mg/g)	Step I		Step II		Step III	
		k_1(mg/g·min$^{1/2}$)	r_1^2	k_2(mg/g·min$^{1/2}$)	r_2^2	k_3(mg/g·min$^{1/2}$)	r_3^2
PAA2	99.60	20.34	0.991	13.59	0.992	4.73	0.958
PAA2-GO-1	142.76	75.10	0.957	4.84	0.957	1.322	0.929
PAA2-GO-2	302.03	76.13	0.979	9.61	0.997	2.41	0.956
PAA2-GO-3	580.99	91.58	0.998	17.51	0.988	4.18	0.989

3.6. Adsorption isotherm

Adsorption properties and equilibrium data, commonly known as adsorption isotherms, describe how pollutants interact with sorbent materials and so are critical in optimizing the use of adsorbents. In order to optimize the design of an adsorption system to remove dye from solutions, it is important to establish the most appropriate correlation for the equilibrium curve.[55] Herein, in order to investigate the adsorption isotherm of the MB, Langmuir and Frenundlich adsorption isotherms were used to investigate the adsorption process.

3.6.1. Langmuir isotherm

The Langmuir adsorption isotherm has been successfully applied to many pollutant adsorption process and has been the most widely used adsorption isotherm for the adsorption of solute from a liquid solution.[56] The Langmuir adsorption was deduced by several hypothesizes: monolayer adsorption; dynamic balance; no interaction between adsorbate molecules; every adsorption sites have the same adsorptive power.[57] The Langmuir equation is obtained as:

$$\frac{C_e}{q_e} = \frac{1}{q_{\max} k_L} + \frac{C_e}{q_{\max}} \qquad (4)$$

where q_e is the mass of the MB adsorbed by the unit mass after the adsorption reaches equilibrium (mg/g); C_e is the equilibrium concentration of the MB (mg/L); q_{max} is the maximal adsorbed amount of the composite hydrogel (mg/g); k_L is the Langmuir adsorption constant.

A plot of C_e/q_e versus C_e shown in Fig. S6 gives a straight line with the slope of $1/q_{max}$ and the intercept $C_e/(q_{max})$; the parameters are shown in Table 5. The values of the correlation coefficient r^2 for the Langmuir equation are 0.997, 0.982, 0.987, and 0.996 for PAA2, PAA2-GO-1, PAA2-GO-2, and PAA2-GO-3, respectively, which indicated that the adsorption of MB on the PAA2/GO composite hydrogels followed the Langmuir adsorption isotherm quite well; thus the adsorption process was monolayer adsorption. The large k_L value of the PAA2/GO composite hydrogels suggested that the PAA2/GO composite hydrogels would be more effective adsorbents for MB and other cationic dyes than the PAA2.

Table 5 The parameters of Langmuir and Freundlich isotherm for the adsorption of MB by the composite hydrogel.

Hybrid hydrogel	Langmuir			Freundlich		
	q_{max}(mg/g)	k_L(L/mg)	r_L^2	n	k_f(L/g)	r_F^2
PAA2	828.57	0.11	0.997	2.06	5.44	0.975
PAA2-GO-1	1034.54	0.24	0.982	2.68	5.75	0.988
PAA2-GO-2	1428.57	0.36	0.987	3.89	5.94	0.996
PAA2-GO-3	2000.00	0.71	0.996	5.06	6.86	0.948

3.6.2. Freundlich isotherm

The Freundlich isotherm is an empirical equation,[58] and its initial form is:

$$q_e = k_F C_e^{1/n} \qquad (5)$$

where k_F is the Freundlich isotherm constant; q_e has the same meaning as that in Eq. (6); 1/n is the influence coefficient of solution concentration to the equilibrium adsorbed amount. The linear form of the Freundlich isotherm equation can be obtained by taking the logarithm of Eq. (5):

$$\ln q_e = k_F + (1/n) \ln C_e \qquad (6)$$

A linear plot was obtained when $\ln q_e$ was plotted against $\ln C_e$, as shown in Fig. S6, and then the parameters (as shown in Table 5) were obtained. It indicated that the adsorption process also fitted this model but the linear correlation coefficients were smaller than those for the Langmuir model. Furthermore, the values of n at the equilibrium (2.06, 2.68, 3.89, and 5.06 for PAA2, PAA2-GO-1, PAA2-GO-2, and PAA2-GO-3,

respectively) were larger than 1, reflecting the favorable adsorption of MB.

3.7. Adsorption of different kinds of water pollutants by the PAA2/GO hydrogels

Besides the interior porous structure, the special adsorption capability of PAA2/GO composite hydrogels could be attributed to the negative charge, which conferred its high adsorb ability to cationic dyes. To further confirm the adsorption character to cationic dyes, the adsorption of MV was further tested. The adsorption capacities of MV by PAA2/GO hydrogels are shown in Fig. 8. It can be observed clearly that the adsorption amount of MV increased obviously when the GO was blended, especially for PAA2-GO-3, which exhibited very high MV absorption amount and almost reached 1050 mg/g. Compared with the above MB adsorption capacities of the PAA2/GO composite hydrogels, the adsorption amount of MV is smaller, which might be resulted from the different dye molecules. In general, the PAA2/GO hydrogels had maintained the good adsorption capacity for cationic dyes. Furthermore, as shown in Fig. 8D, the excellent MV desorption ratios in acidic aqueous solution indicated that the total desorption ratios could reach almost 100 % for all the hydrogels in acidic aqueous solution.

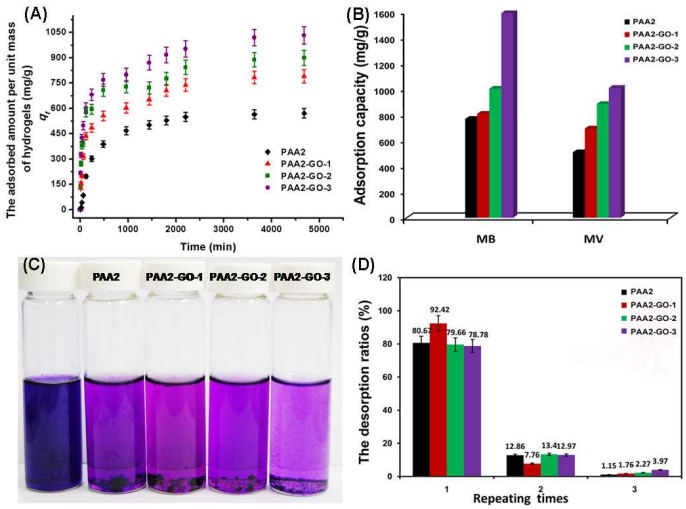

Fig. 8. (a) The adsorption capacity for MV by PAA2/GO hydrogels at equilibrium. 1 mg hydrogel is applied in 50 mL 100 μmol/L pollutant solutions at 25±1 °C, and the pH value of the solution is 6.6. Data are expressed as the mean ±S.D. of three independent measurements. (b) The total adsorbed MV and MB amounts per unit mass of PAA2, PAA2-GO-1, PAA2-GO-2, and PAA2-GO-3 at equilibrium. (c) Photograph of the adsorption of MV at equilibrium. (d) The desorption ratios of the adsorbed MB in acidic aqueous solutions. The desorption process was repeated for three times, and each time continued 24h. Data are expressed as the mean ±S.D. of three independent measurements.

Heavy metal ions are also toxins that are harmful for environment, thus we examined the removal capacity of heavy metal ions by PAA2/GO composite hydrogels. The adsorption processes of Cu^{2+} and Pb^{2+} to the PAA2/GO hydrogels are shown in Fig. 9. It can be seen that the adsorption of Cu^{2+} and Pb^{2+} onto the hydrogels increased dramatically within the first 2 h, and then increased slowly and took 48 h for Cu^{2+} and Pb^{2+} to reach adsorption equilibrium. It was obviously shorter than that of MB and MV since the metal ions have small diameters and large diffusion coefficients than cationic molecules. The maximum adsorption capacities of PAA2, PAA2-GO-1, PAA2-GO-2 and PAA2-GO-3 for Cu^{2+} are 90, 122, 140, and 158 mg/g, respectively; and the adsorption amounts for Pb^{2+} are 306, 339, 405 and 509 mg/g, respectively. These adsorption capacities are comparable with the reported PAA composite hydrogels.[59] The strong adsorption capacity of the PAA2/GO composite hydrogels should be resulted from the synergistic effects of the static electrical attraction and the surface complexation between the carboxyl/hydroxyl groups and heavy metal ions. Herein, the facile and environmental self-assembled PAA/GO hydrogels could act as promising adsorbents for the removal of heavy metal ions in industry.

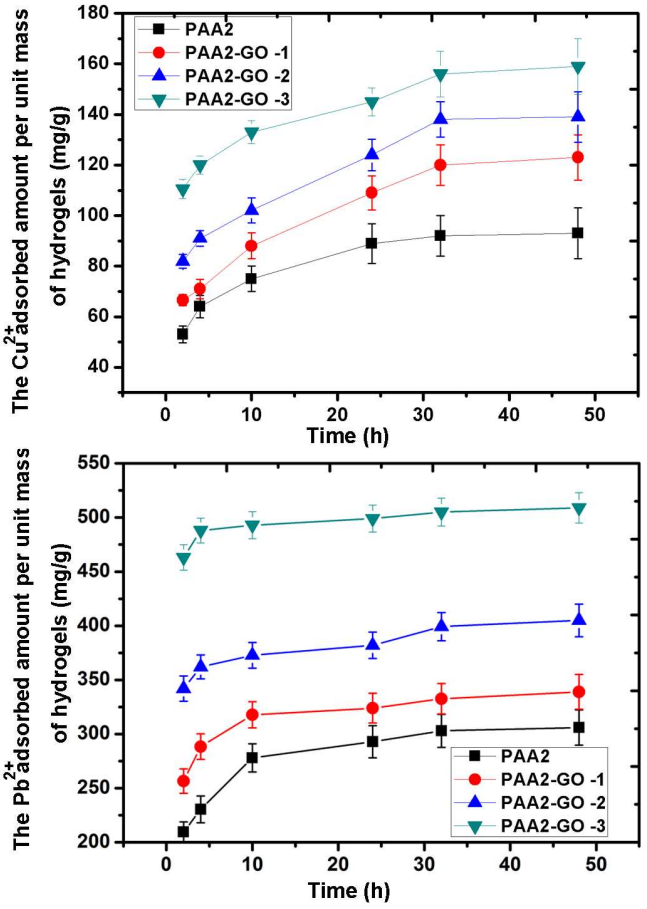

Fig. 9. (a) Time-dependent adsorption of Cu^{2+} ions on the PAA2/GO hydrogels. (b) Time-dependent adsorption of Pb^{2+} ions on the PAA2/GO hydrogels. Initial concentration is 1 mmol/L and at 25 °C.

4. Conclusion

In this study, GO interpenetrated PAA composite hydrogels as high-efficient adsorbents were prepared and systematically studied for the first time. The mediating ability of GO on inner structure and adsorption capacities are examined by two types of PAA hydrogels. The results indicated that the prepared PAA/GO composite hydrogels own well-defined and

interconnected 3D porous network, which allows the adsorbate molecules to diffuse easily into the absorbent. The adsorption experiments indicated that the obtained interconnected polymeric composite hydrogels can efficiently remove cationic dyes and heavy metal ions from wastewater; the highest adsorption capacity of the prepared PAA2/GO composite hydrogels can reach as high as 1600 mg/g, which is comparable to most of reported adsorption capacity and make the composite hydrogels present great potential in the treatment of environmental toxins. Moreover, the initial concentration, pH value, desorption ratio, dynamic kinetics and isotherms of the MB adsorption processes of the prepared PAA2/GO composite hydrogels were also studied in detail. The experimental data of MB adsorption fitted the pseudo-second-order kinetic model and the Langmuir isotherm very well, and the adsorption process was controlled by the intraparticle diffusion. Moreover, due to its facile preparation and low-cost, the GO interpenetrated PAA composite hydrogels may function as promising adsorbents for the application in wastewater treatment, and this method might also be extended to improve the adsorption capacity of other polymeric hydrogels, such as PSS, PAM, and etc.

Acknowledgements

This work was financially sponsored by the National Natural Science Foundation of China (No. 51173119, and 51225303), and Program for Changjiang Scholars and Innovative Research Team in University (IRT1163). We should also thank our laboratory members for their generous help, and gratefully acknowledge the help of Ms H. Wang, of the Analytical and Testing Center at Sichuan University, for the SEM images. We sincerely acknowledge the financial assistance of visiting research program in University of Michigan by the China Scholarship Council (CSC).

Notes and references

[a] *College of Polymer Science and Engineering, State Key Laboratory of Polymer Materials Engineering, Sichuan University, Chengdu 610065, China*
[b] *Department of Chemical Engineering, Department of Biomedical Engineering, University of Michigan, Ann Arbor, Michigan, 48109, USA*
[c] *Department of Nephrology, West China Hospital, Sichuan University, Chengdu 610041, China*
** Corresponding author.*
Tel: +86-28-85400453, Fax: +86-28-85405402, E-mail: (T. Zhou) zhoutaopoly@scu.edu.cn; (C.S. Zhao) zhaochsh70@163.com or zhaochsh70@scu.edu.cn

† Electronic Supplementary Information (ESI) available: [Detailed information of GO preparation method and characterization, components, SEM images, and MB adsorption amount of PAA1/GO composite hydrogels, adsorption isotherm of MB onto PAA2/GO hybrid hydrogel]. See DOI: 10.1039/b000000x/

1. M.-S. Chiou, P.-Y. Ho and H.-Y. Li, *"J. Chin. Inst. Chem. Eng, "* 2003, 34, 625-634.
2. Y. F. Lin, H. W. Chen, P. S. Chien, C. S. Chiou and C. C. Liu, *J. Hazard. Mater.* , 2011, 185, 1124-1130.
3. M. A. Shannon, P. W. Bohn, M. Elimelech, J. G. Georgiadis, B. J. Mariñas and A. M. Mayes, *Nature*, 2008, 452, 301-310.
4. W. Kamiński and Z. Modrzejewska, *Sep. Sci. Technol.* , 1997, 32, 2659-2668.
5. P. J. Cyr, R. P. S. Suri and E. D. Helmig, *Water Res.* , 2002, 36, 4725-4734.
6. J. H. Lee, D. I. Song and Y. W. Jeon, *Sep. Sci. Technol.* , 1997, 32, 1975-1992.
7. N. Frini-Srasra and E. Srasra, *Desalination*, 2010, 250, 26-34.
8. J. Pan, X. Zou, X. Wang, W. Guan, C. Li, Y. Yan and X. Wu, *Chem. Eng. J.* , 2011, 166, 40-48.
9. V. Vimonses, S. Lei, B. Jin, C. W. K. Chow and C. Saint, *Chem. Eng. J.* , 2009, 148, 354-364.
10. B. O. Yoon, S. Koyanagi, T. Asano, M. Hara and A. Higuchi, *J. Membr. Sci.* , 2003, 213, 137-144.
11. D. R. Kioussis, F. W. Wheaton and P. Kofinas, *Aquacult. Eng.* , 1999, 19, 163-178.
12. H.-P. Cong, X.-C. Ren, P. Wang and S.-H. Yu, *Acs Nano*, 2012, 6, 2693-2703.
13. H.-L. Jiang, B. Liu, Y.-Q. Lan, K. Kuratani, T. Akita, H. Shioyama, F. Zong and Q. Xu, *J. Am. Chem. Soc.* , 2011, 133, 11854-11857.
14. J. Wu, J. Lu, J. Hu, Y. Gao, Q. Ma and Y. Ju, *RSC Advances*, 2013, 3, 24906-24909.
15. F. Gnanaprakasam Thankam and J. Muthu, *RSC Advances*, 2013, 3, 24509-24520.
16. F. Liu, S. Chung, G. Oh and T. S. Seo, *ACS Appl. Mater. Interfaces* 2011, 4, 922-927.
17. K. Saeed, S. Haider, T.-J. Oh and S.-Y. Park, *J. Membr. Sci.* , 2008, 322, 400-405.
18. E. Salehi, S. S. Madaeni, L. Rajabi, A. A. Derakhshan, S. Daraei and V. Vatanpour, *Chem. Eng. J.* , 2013, 215–216, 791-801.
19. M. Zhang, B. Gao, X. Cao and L. Yang, *RSC Advances*, 2013, 3, 21099-21105.
20. Y. Xu, K. Sheng, C. Li and G. Shi, *ACS nano*, 2010, 4, 4324-4330.
21. X. Zhang, C. Cheng, J. Zhao, L. Ma, S. Sun and C. Zhao, *Chem. Eng. J.* , 2013, 215–216, 72-81.
22. M. S. Mauter and M. Elimelech, *Environmental Science & Technology*, 2008, 42, 5843-5859.
23. Y. Yao, S. Miao, S. Yu, L. Ping Ma, H. Sun and S. Wang, *J. Colloid Interface Sci.* , 2012, 379, 20-26.
24. X. Gu, Y. Ning, Y. Yang and C. Wang, *RSC Advances*, 2014, 4, 3211-3218.
25. N. Lu, J. Liu, J. Li, Z. Zhang, Y. Weng, B. Yuan, K. Yang and Y. Ma, *Journal of Materials Chemistry B*, 2014, 2, 3791-3798.
26. R. Justin and B. Chen, *Journal of Materials Chemistry B*, 2014, 2, 3759-3770.
27. W. Zhang, C. Zhou, W. Zhou, A. Lei, Q. Zhang, Q. Wan and B. Zou, *Bulletin of environmental contamination and toxicology*, 2011, 87, 86-90.
28. Y. Zhu, S. Murali, W. Cai, X. Li, J. W. Suk, J. R. Potts and R. S. Ruoff, *Adv. Mater.* , 2010, 22, 3906-3924.
29. V. Chandra and K. S. Kim, *Chem. Commun.* , 2011, 47, 3942-3944.
30. R. Li, L. Liu and F. Yang, *Chem. Eng. J.* , 2013, 229, 460-468.
31. L. Yang, Z. Li, G. Nie, Z. Zhang, X. Lu and C. Wang, *Appl. Surf. Sci.* , 2014, 307, 601-607.

32. C. Cheng, S. Li, J. Zhao, X. Li, Z. Liu, L. Ma, X. Zhang, S. Sun and C. Zhao, *Chem. Eng. J.* , 2013, 228, 468-481.
33. V. H. Luan, J. S. Chung, E. J. Kim and S. H. Hur, *Chem. Eng. J.* , 2014, 246, 64-70.
34. Y. Wang, P. Zhang, C. F. Liu and C. Z. Huang, *RSC Advances*, 2013, 3, 9240-9246.
35. Y. Zeng, L. Qiu, K. Wang, J. Yao, D. Li, G. P. Simon, R. Wang and H. Wang, *RSC Advances*, 2013, 3, 887-894.
36. J. Fan, Z. Shi, M. Lian, H. Li and J. Yin, *Journal of Materials Chemistry A*, 2013, 1, 7433-7443.
37. A. He, B. Lei, C. Cheng, S. Li, L. Ma, S. Sun and C. Zhao, *RSC Advances*, 2013, 3, 22120-22129.
38. Y. Yang, Y. Xie, L. Pang, M. Li, X. Song, J. Wen and H. Zhao, *Langmuir*, 2013, 29, 10727-10736.
39. S. Faghihi, M. Gheysour, A. Karimi and R. Salarian, *J. Appl. Phys.* , 2014, 115, -.
40. Z. Jiang, Q. Li, M. Chen, J. Li, J. Li, Y. Huang, F. Besenbacher and M. Dong, *Nanoscale*, 2013, 5, 6265-6269.
41. Y. Huang, M. Zeng, J. Ren, J. Wang, L. Fan and Q. Xu, *"Colloids Surf., A "*, 2012, 401, 97-106.
42. J. Shen, B. Yan, T. Li, Y. Long, N. Li and M. Ye, *Soft Matter*, 2012, 8, 1831-1836.
43. J. Kim, L. J. Cote, F. Kim, W. Yuan, K. R. Shull and J. Huang, *J. Am. Chem. Soc.* , 2010, 132, 8180-8186.
44. H. Zhou, C. Cheng, H. Qin, L. Ma, C. He, S. Nie, X. Zhang, Q. Fu and C. Zhao, *Polymer Chemistry*, 2014, 5, 3563-3575.
45. C. Cheng, S. Li, S. Nie, W. Zhao, H. Yang, S. Sun and C. Zhao, *Biomacromolecules*, 2012, 13, 4236-4246.
46. C. Cheng, S. Nie, S. Li, H. Peng, H. Yang, L. Ma, S. Sun and C. Zhao, *Journal of Materials Chemistry B*, 2013, 1, 265-275.
47. N. Zhang, R. Li, L. Zhang, H. Chen, W. Wang, Y. Liu, T. Wu, X. Wang, W. Wang and Y. Li, *Soft Matter*, 2011, 7, 7231-7239.
48. M. Min, L. Shen, G. Hong, M. Zhu, Y. Zhang, X. Wang, Y. Chen and B. S. Hsiao, *Chem. Eng. J.* , 2012, 197, 88-100.
49. M. Doğan, Y. Özdemir and M. Alkan, *Dyes Pigm.* , 2007, 75, 701-713.
50. S. S. Gupta and K. G. Bhattacharyya, *J. Hazard. Mater.* , 2006, 128, 247-257.
51. G. Crini, H. N. Peindy, F. Gimbert and C. Robert, *Sep. Purif. Technol.* , 2007, 53, 97-110.
52. C. Cheng, J. Deng, B. Lei, A. He, X. Zhang, L. Ma, S. Li and C. Zhao, *J. Hazard. Mater.* , 2013, 263, Part 2, 467-478.
53. E. N. El Qada, S. J. Allen and G. M. Walker, *Chem. Eng. J.* , 2006, 124, 103-110.
54. F.-C. Wu, R.-L. Tseng and R.-S. Juang, *Chem. Eng. J.* , 2009, 153, 1-8.
55. G. Crini, H. N. Peindy, F. Gimbert and C. Robert, *Sep. Purif. Technol.* , 2007, 53, 97-110.
56. B. H. Hameed, A. L. Ahmad and K. N. A. Latiff, *Dyes Pigm.* , 2007, 75, 143-149.
57. B. Hameed, A. Ahmad and K. Latiff, *Dyes Pigm.* , 2007, 75, 143-149.
58. C. Cheng, L. Ma, J. Ren, L. Li, G. Zhang, Q. Yang and C. Zhao, *Chem. Eng. J.* , 2011, 171, 1132-1142.
59. J. Zhang and A. Wang, *Journal of Chemical & Engineering Data*, 2010, 55, 2379-2384.

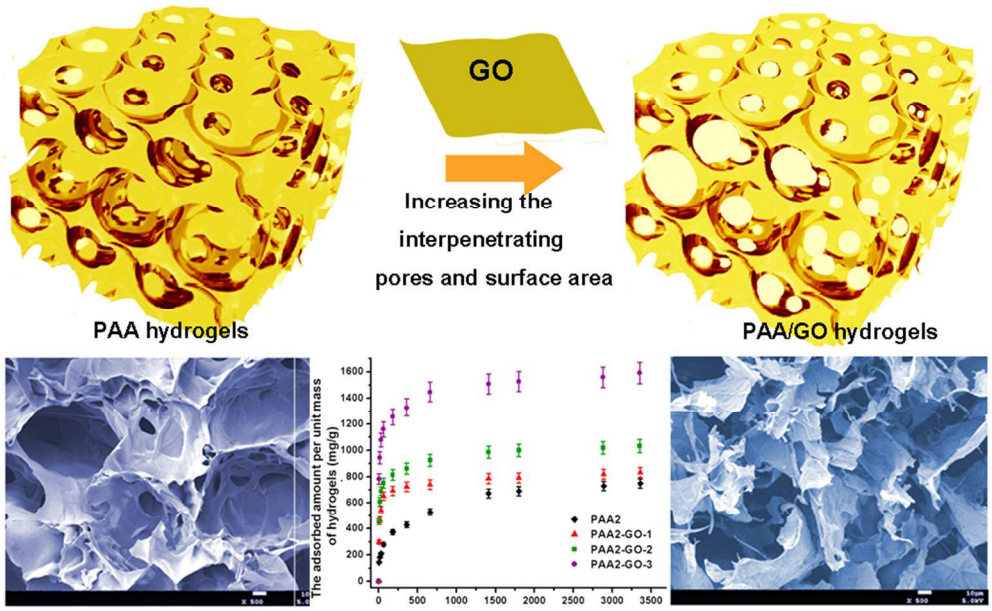

In this study, synthetic GO interpenetrated PAA composite hydrogels were prepared and systematically studied as 3D high-efficient adsorbents for water treatment
88x54mm (300 x 300 DPI)